ELSEVIER

Signal Processing 43 (1995) 149–168

SIGNAL PROCESSING

Smoothed pseudo-Wigner distribution, Choi–Williams distribution, and cone-kernel representation: Ambiguity-domain analysis and experimental comparison ☆

Franz Hlawatsch[a,*], Thulasinath G. Manickam[b], Rüdiger L. Urbanke[c], William Jones[d]

[a] *Institut für Nachrichtentechnik und Hochfrequenztechnik, Technische Universität Wien, Gusshausstrasse 25/389, A-1040 Vienna, Austria*

[b] *Department of Electrical Engineering, University of Rhode Island, Kingston, RI 02881, USA*

[c] *Department of Electrical Engineering, Washington University, St. Louis, MO 63130, USA*

[d] *USCG Research and Development Center, 1082 Shennecossett Rd, Groton, CT 06340, USA*

Received 22 July 1993; revised 28 November 1994

Abstract

The smoothed pseudo-Wigner distribution, the Choi–Williams distribution, and the cone-kernel representation are three time–frequency representations (TFRs) which feature an attenuation of cross (interference) terms as compared with the Wigner distribution. In this paper, we use an analysis of ambiguity-domain weighting functions for comparing the interference attenuation and time–frequency concentration properties of the three TFRs. These properties are then further investigated by studying the results obtained for a set of simple two-component signals. This analysis shows important effects and performance limitations whose understanding is essential for a practical application of the TFRs.

Zusammenfassung

Die geglättete Pseudo-Wignerverteilung, die Choi–Williams-Verteilung und die Cone-Kernel-Darstellung sind Zeit–Frequenz-Signaldarstellungen, deren Kreuz- bzw. Interferenzterme i.a. kleiner sind als jene der Wignerverteilung. In der vorliegenden Arbeit werden mittels einer Analyse im "Ambiguitätsbereich" die Interferenzunterdrückungs- und Zeit–Frequenz-Konzentrationseigenschaften der drei Zeit–Frequenz-Signaldarstellungen verglichen. Zur weiteren Untersuchung dieser Eigenschaften werden die für einfache zweikomponentige Signale erhaltenen Ergebnisse betrachtet. Diese Analyse zeigt die Existenz wichtiger Effekte und Beschränkungen der Leistungsfähigkeit, deren Verständnis für eine praktische Anwendung der Zeit–Frequenz-Signaldarstellungen wesentlich ist.

Résumé

La distribution pseudo-Wigner lissée, la distribution de Choi–Williams, et la représentation par noyau en cône sont trois représentations temps–fréquence (TFR) caractérisées par une atténuation des termes d'interférence croisée par rapport à la distribution de Wigner. Dans cet article, nous utilisons une analyse des fonctions de pondération dans le domaine de l'ambiguïté pour comparer l'atténuation de l'interférence et les propriétés de concentration temps–fréquence des trois TFR. Ces propriétés sont ensuite analysées plus en détail par l'étude des résultats obtenus sur un ensemble des signaux simples à

☆ This work was supported in part by the Fonds zur Förderung der wissenschaftlichen Forschung under Grant J0530-TEC.

* Corresponding author. E-mail: fhlawats@email.tuwien.ac.at.

SSDI 0165-1684(94)00150-2

deux composantes. Cette analyse montre des effets importants et des limitations de performances dont la compréhension est essentielle pout une application pratique des TFR.

Keywords: Signal analysis; Time–frequency representations; Smoothed Wigner distributions; Choi–Williams distribution; Cone-kernel representation; cross terms

1. Introduction

Quadratic time–frequency representations (TFRs) [7, 12, 4, 11, 1] are powerful tools for the analysis of signals. Among quadratic TFRs with "energetic" interpretation, the Wigner distribution (WD) [3, 12, 13, 15]

$$W_x(t,f) = \int_\tau x\left(t+\frac{\tau}{2}\right) x^*\left(t-\frac{\tau}{2}\right) e^{-j2\pi f\tau}\, d\tau \qquad (1)$$

can be regarded as theoretically optimal in that it satisfies a maximum number of desirable mathematical properties and features optimal time–frequency (TF) concentration.[1] However, the cross or interference terms (ITs) of the WD [13] are often a grave problem in practical applications, especially if a WD outcome is to be visually analyzed by a human signal analyst. Since ITs are oscillatory, they can be attenuated by means of a smoothing operation which corresponds to the convolution of the WD with a 2-D "smoothing kernel" [7, 12, 13]. Quite generally, the smoothing tends to produce the following effects:

1. a (desired) partial attenuation of ITs;
2. an (undesired) broadening of signal terms, i.e., a loss of TF concentration;
3. a (sometimes undesired) loss of some of the nice mathematical properties of the WD.

The design of a "good" smoothing kernel is hence an attempt to achieve effect 1 while avoiding, as far as possible, effect 2 and, if mathematical properties are important, also effect 3.

The classical spectrogram (squared magnitude of the short-time Fourier transform) is a smoothed WD [3, 7, 12, 13]. The spectrogram smoothing is quite extensive and suffers from an unavoidable tradeoff between time concentration and frequency concentration. Moreover, the spectrogram does not satisfy most of the mathematical properties of the WD. This motivates the interest in other smoothed WDs which represent an alternative to the spectrogram.

1.1. Smoothed pseudo-WD, Choi–Williams distribution, and cone-kernel representation

The *pseudo-Wigner distribution* [3] has been defined as a short-time WD using a running analysis window. The pseudo-WD is a smoothed WD which, however, implements only a smoothing in the frequency direction. Thus, the WD's time concentration is preserved but ITs oscillating in the time direction are not attenuated. This restriction is removed in the *smoothed pseudo-Wigner distribution* (SPWD) [8, 6, 13] which is a pseudo-WD with an additional smoothing in the time direction. The SPWD is conceptually simple, and it allows both an easy and flexible choice of the smoothing characteristics and an efficient implementation. However, like the spectrogram, it does not satisfy most of the mathematical properties satisfied by the WD (see Table 1).

A TFR which retains many desirable mathematical properties and yet attains a partial attenuation of ITs is the *Choi–Williams distribution* (CWD) [2, 16]. In particular, the CWD satisfies the marginal properties and is thus an "energy distribution". On the other hand, it has been shown that the validity of the marginal properties places a limit on the IT attenuation of any TFR [13]. A generalization of the CWD, the family of "reduced interference distributions" [16], satisfies also the finite-support properties. Other extensions of the CWD (e.g., the *generalized exponential distribution* and the *Butterworth distribution*) are introduced in [20, 5].

The *cone-kernel representation* (CKR) [21, 19] has been designed specifically to achieve good TF concentration and good IT attenuation in the case of multiple sinusoidal bursts with quasi-stationary instantaneous frequencies, as encountered in voiced speech signals. The CKR satisfies the temporal finite-support property (see Table 1) and is yet capable of attenuating ITs

[1] In (1) and subsequent equations, $x(t)$ is the signal to be analyzed, t and f denote time and frequency, respectively, and integrations go from $-\infty$ to ∞.

Table 1
Mathematical properties of the smoothed pseudo-WD (SPWD), the Choi–Williams distribution (CWD), and the cone-kernel representation (CKR). The properties are defined in [12, Table II]

Property	SPWD	CWD	CKR
P_1: real-valuedness	√ if $g(t) \in \mathbb{R}$	√	√ if $g(-t) = g(t)$
P_2: time-shift invariance	√	√	√
P_3: frequency-shift invariance	√	√	√
P_4: time marginal		√	
P_5: frequency marginal		√	
P_6: time moments		√	
P_7: frequency moments		√	
P_8: time–frequency scaling		√	
P_9: instantaneous frequency		√	
P_{10}: group delay		√	
P_{11}: finite time support			√
P_{12}: finite frequency support			
P_{13}: Moyal's formula/unitarity			
P_{14}: convolution			
P_{15}: multiplication			
P_{16}: Fourier transform		√	
P_{17}: chirp convolution			
P_{18}: chirp multiplication			

oscillating in the time direction. Most other properties are not satisfied; in particular, the CKR is not an "energy distribution" since its integral over the entire TF plane is always zero.

1.2. Motivation and outline of paper

This paper provides a comparative discussion of the SPWD, CWD, and CKR with regard to TF concentration and interference geometry/attenuation. It also provides an objective experimental comparison of the three TFRs by contrasting their results for simple but fundamental, two-component signals.

Since the CWD and CKR have been the subject of a number of interesting papers that have yielded valuable results and insights [2, 5, 9, 10, 13, 14, 16–21] it is worthwhile to point out in which respects this paper is different from previous work, which new aspects are discussed in the paper, and why these aspects are relevant:

- Perhaps most important, this paper seems to be the first discussion that compares the CWD and CKR with the SPWD. While the CWD and CKR have been introduced some years after the SPWD, and have been claimed to achieve a performance improvement over existing techniques, a detailed comparison with the SPWD has not been given so far (except for very brief and limited comparisons in [12, 9]). Instead, the CWD and CKR have been compared with the WD, pseudo-WD, and spectrogram [2, 16–19, 21]. However, such a comparison is not too meaningful since the WD and pseudo-WD are well known to implement too little smoothing (the WD has no smoothing at all whereas the pseudo-WD smooths only in the frequency direction), and the spectrogram generally implements too much smoothing. Hence, it is very easy to outperform the WD and pseudo-WD with respect to IT attenuation, and the spectrogram with respect to TF concentration.
- We provide a systematic discussion of two important performance aspects, namely, TF concentration and IT attenuation. Our analysis of the properties of TF concentration and IT attenuation will be based on the "ambiguity domain" [6, 2, 11, 13] where the WD smoothing is characterized by a simple kernel multiplication, whose effects on signal terms and ITs are easily understood. Again, it seems that a detailed ambiguity-domain comparison of the SPWD, CWD, and CKR has not been performed so far.
- We give an objective and detailed comparison of the SPWD, CWD, and CKR results obtained for

a set of simple two-component signals. These signals comprise constant-frequency components, impulsive components, Gaussians, chirp components, and quadratic FM components. While many papers have concentrated on specific signal types where the advantages of a given TFR are most pronounced, we have attempted to select signals that are diverse enough to minimize any undesired bias. Also, we have purposely used simple synthetic signals since only these allow an easy analysis in the ambiguity domain and thus yield insights into the basic behavior of a TFR regarding TF concentration and IT geometry/attenuation. These insights are absolutely necessary for correctly interpreting the TFR results obtained for more complicated real-world signals.

2. Ambiguity-domain analysis of IT attenuation and TF concentration

In this section, we discuss and compare the IT attenuation and TF concentration properties of the SPWD, CWD, and CKR by means of an analysis in the "ambiguity domain".

2.1. The ambiguity domain

The smoothed WDs considered in this paper can be written as a convolution of the WD with a real-valued smoothing kernel $\psi_T(t,f)$ [3, 7, 12, 13],

$$T_x(t,f) = \int_{t'}\int_{f'} \psi_T(t-t', f-f') W_x(t',f')\,\mathrm{d}t'\,\mathrm{d}f'. \tag{2}$$

Introducing the *ambiguity function* (AF)

$$A_x(\tau,\nu) = \int_t x\left(t+\frac{\tau}{2}\right) x^*\left(t-\frac{\tau}{2}\right) \mathrm{e}^{-\mathrm{j}2\pi\nu t}\,\mathrm{d}t,$$

which is essentially the Fourier transform of the WD, the smoothed WD $T_x(t,f)$ defined in (2) can also be written as [2, 4, 6, 7, 11–13]

$$T_x(t,f) = \int_\tau\int_\nu [\Psi_T(\tau,\nu) A_x(\tau,\nu)]\,\mathrm{e}^{\mathrm{j}2\pi(t\nu - f\tau)}\,\mathrm{d}\tau\,\mathrm{d}\nu, \tag{3}$$

i.e., as the inverse Fourier transform of the signal's AF multiplied (weighted) by a *weighting function* $\Psi_T(\tau,\nu)$. This weighting function is the Fourier transform of the smoothing function $\psi_T(t,f)$ in (2),

$$\Psi_T(\tau,\nu) = \int_t\int_f \psi_T(t,f)\mathrm{e}^{-\mathrm{j}2\pi(\nu t - \tau f)}\,\mathrm{d}t\,\mathrm{d}f.$$

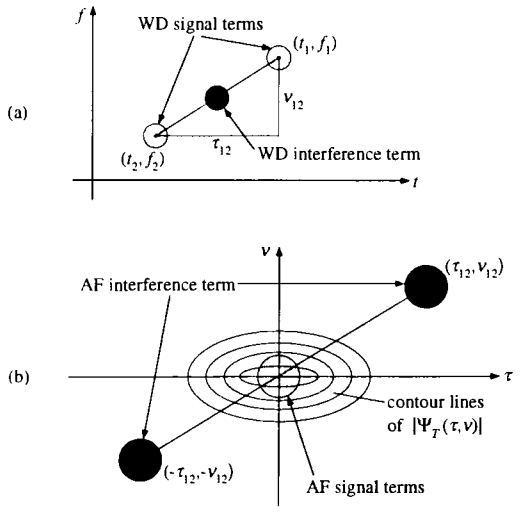

Fig. 1. (a) Basic interference term geometry of the WD. (b) Ambiguity-domain analysis of IT attenuation.

In the ambiguity domain defined by (3), the convolution in (2) is replaced by a simple multiplication. Consequently, many properties of the smoothed WD $T_x(t,f)$ can now be discussed very easily in terms of the shape of the weighting function $\Psi_T(\tau,\nu)$. Evidently, the smoothness of $\psi_T(t,f)$ implies that the weighting function $\Psi_T(\tau,\nu)$ is concentrated around the origin of the (τ,ν)-plane. Indeed, the weighting function can be interpreted as the transfer function of a two-dimensional lowpass filter.

Let us consider the basic situation of a signal that has energy around two points (t_1,f_1) and (t_2,f_2) in the TF plane. The WD of such a signal will contain two "signal terms" around (t_1,f_1) and (t_2,f_2) and an IT around the center point (t_{12},f_{12}) with $t_{12} = (t_1+t_2)/2$ and $f_{12} = (f_1+f_2)/2$. The IT is oscillatory and partly negative; the direction of fastest oscillation is perpendicular to the line connecting the two "signal points" (t_1,f_1) and (t_2,f_2) [13]. This geometry is illustrated in Fig. 1(a).

Just as the WD, the AF contains two "signal terms" and an IT. The AF's signal terms are located around the origin of the (τ,ν)-plane. In contrast, the AF's IT can be shown to be located around the two "lag

points" (τ_{12}, ν_{12}) and $(-\tau_{12}, -\nu_{12})$, where $\tau_{12} = t_1 - t_2$ and $\nu_{12} = f_1 - f_2$ are the time and frequency differences, respectively, of the signal points (t_1, f_1) and (t_2, f_2). Hence, it follows with (3) that the attenuation of the IT depends on the value of $|\Psi_T(\tau, \nu)|$ around (τ_{12}, ν_{12}). This is illustrated in Fig. 1(b). Good IT attenuation, even for signal components closely spaced in the TF plane (i.e., involving small lags τ_{12} and ν_{12}), is achieved if $\Psi_T(\tau, \nu)$ is very narrow around the origin of the (τ, ν)-plane. On the other hand, if $\Psi_T(\tau, \nu)$ is too narrow, the AF signal terms will in many cases be truncated by the weighting function $\Psi_T(\tau, \nu)$. This truncation in the ambiguity domain corresponds to a broadening of the WD signal terms and, hence, a loss of TF concentration in the smoothed WD. It is thus clear that the two goals of good IT attenuation and good TF concentration are essentially contradictory.

While there exists a fundamental general trade-off between IT attenuation and TF concentration, the weighting function $\Psi_T(\tau, \nu)$ can be designed to achieve good overall performance for specific classes of signals. In the following, we shall take a closer look at the weighting functions of the SPWD, CWD, and CKR, and we shall attempt to find out for which situations these weighting functions are best suited, and what performance limitations are to be expected. In Section 3, these theoretical results will be illustrated by means of computer simulations. As stated before, our main interest is in the shape of the ambiguity-domain weighting function $\Psi_T(\tau, \nu)$ and its implications with respect to IT attenuation and TF concentration characteristics. These characteristics are the most important ones if the application is the visual analysis of TFR results by a human analyst. Here, mathematical properties are of secondary or no importance,[2] and the main requirement is that ITs are sufficiently attenuated with only moderate loss of the TF concentration of the desired signal terms.

2.2. The smoothed pseudo-WD

The *smoothed pseudo-Wigner distribution* (SPWD) is defined as a time-smoothed short-time version of the WD employing a running analysis window $h(t)$ and a time-smoothing window $g(t)$ [8, 6, 13, 12]. The SPWD's ambiguity-domain weighting function is

$$\Psi_{\mathrm{SPWD}}(\tau, \nu) = \phi_h(\tau) G(\nu) ,$$

where $\phi_h(\tau) = h\left(\frac{1}{2}\tau\right) h^*\left(-\frac{1}{2}\tau\right)$ and $G(\nu)$ is the Fourier transform of $g(t)$. An example is given in Fig. 2(a). The weighting function is a separable function whose factors $\phi_h(\tau)$ and $G(\nu)$ depend on the analysis window $h(t)$ and the time-smoothing window $g(t)$, respectively. The amounts of time smoothing and frequency smoothing can be controlled very easily and independently by suitably choosing the lengths of the windows $g(t)$ and $h(t)$, respectively: a longer $g(t)$ yields more time smoothing and a longer $h(t)$ yields less frequency smoothing.

For usual windows $g(t)$ and $h(t)$, the SPWD smoothing corresponds to a very simple two-dimensional lowpass filter. The weighting function $\Psi_{\mathrm{SPWD}}(\tau, \nu)$ will typically be similar to a 2-D Gaussian function. Because of the simple shape of the weighting function, the IT attenuation and TF concentration of the SPWD will not depend too much on the detailed TF structure of the signal under analysis. However, the SPWD does not satisfy most of the mathematical properties of the WD (see Table 1). The CWD and the CKR, to be discussed next, implement a more sophisticated WD filtering.

2.3. The Choi–Williams distribution

The *Choi–Williams distribution* (CWD) [2, 5, 9, 10, 12–14, 16, 20] is a smoothed WD that retains a large number of desirable mathematical properties (see Table 1). In particular, the CWD satisfies the marginal properties and is thus an "energy distribution". It is characterized by a weighting function

$$\Psi_{\mathrm{CWD}}(\tau, \nu) = \exp\left[-\frac{(2\pi\tau\nu)^2}{\sigma}\right] ,$$

where σ is a positive parameter controlling the concentration of $\Psi_{\mathrm{CWD}}(\tau, \nu)$ around the origin of the (τ, ν)-plane and, hence, the overall amount of smoothing. A larger σ yields a broader $\Psi_{\mathrm{CWD}}(\tau, \nu)$, corresponding to less smoothing. An independent choice of the amounts of time smoothing and frequency smoothing is not possible.

[2] For completeness, the mathematical properties of the SPWD, CWD, and CKR are compared in Table 1.

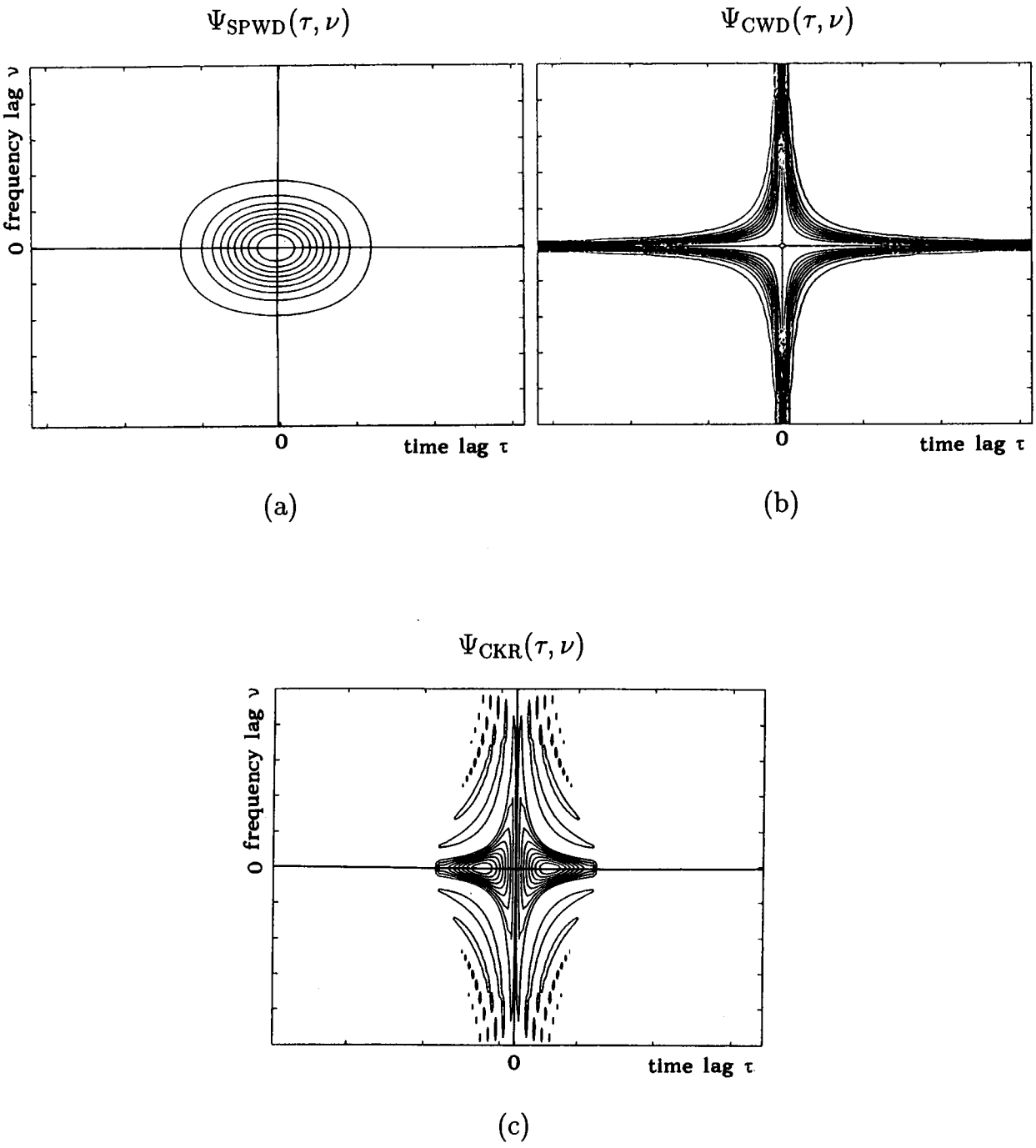

Fig. 2. Ambiguity-domain weighting functions $\Psi_T(\tau,\nu)$ of (a) the SPWD, (b) the CWD, and (c) the CKR.

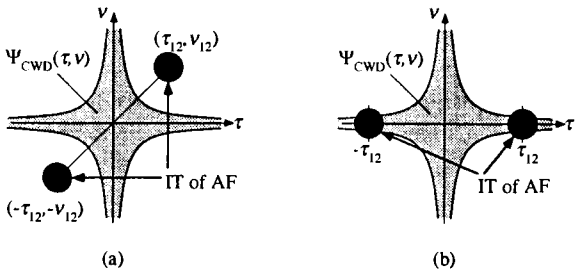

Fig. 3. Ambiguity-domain analysis of the IT attenuation in the CWD. (a) Case $\tau_{12} \neq 0$ and $\nu_{12} \neq 0$, (b) case $\tau_{12} \neq 0$ and $\nu_{12} = 0$.

Since the weighting function $\Psi_{CWD}(\tau, \nu)$ depends only on the *product* of τ and ν, it has a characteristic cross shape (see Fig. 2(b)). Specifically,

$$\Psi_{CWD}(\tau, 0) = \Psi_{CWD}(0, \nu) = 1 ,$$

i.e., the CWD weighting function does not decay on the τ- or ν-axis. This behavior (which is necessary for the marginal properties to be satisfied) entails a characteristic limitation of IT attenuation. In fact, the CWD must be expected to yield poor IT attenuation if the interfering "signal points" occur at the same time or at the same frequency. In the first case, there is $t_1 = t_2$ or $\tau_{12} = 0$, which means that the AF's IT falls on the ν-axis where $\Psi_{CWD}(0, \nu) = 1$. In the second case, we have $f_1 = f_2$ or $\nu_{12} = 0$ so that the AF's IT falls on the τ-axis where $\Psi_{CWD}(\tau, 0) = 1$.

Fig. 3 contrasts the case of $\tau_{12} \neq 0$ and $\nu_{12} \neq 0$ resulting in good IT attenuation and the case $\nu_{12} = 0$ resulting in poor IT attenuation. In the latter case, the AF's IT is truncated by the weighting function, which causes a broadening of the CWD's IT in the time direction. In fact, while the height of the CWD's IT is reduced (as compared to the WD's IT), the time spread of the CWD's IT is increased in proportion. This behavior is consistent with the second marginal property which implies that the CWD's integral with respect to time equals the corresponding integral of the WD. Hence, a reduction of IT height is paid for by an increase of the IT's time spread, such that the IT's time integral remains unchanged. Of course, an analogous discussion applies to the case $\tau_{12} = 0$: here, the IT oscillates in the time direction, and it is spread out in the frequency direction.

From this ambiguity-domain analysis, it follows that the CWD will feature residual ITs whenever the signal components overlap either with respect to time or with respect to frequency. These residual ITs are constrained to the overlap intervals; they are reduced in height but increased in width (as compared to the ITs of the WD). We emphasize that similar residual ITs will be observed in *any* TFR that satisfies the marginal properties. This is especially true for the "reduced interference distributions" [16] which have cross-shaped weighting functions as well.

The CWD's TF concentration depends heavily on the specific signal. For good TF concentration, the AF signal terms must fall essentially into the "pass region" of the cross-shaped weighting function $\Psi_{CWD}(\tau, \nu)$. Consequently, the TF concentration will be very good for either an impulsive signal or a constant-frequency signal since here the AF is concentrated along the τ-axis and the ν-axis, respectively where $\Psi_{CWD}(\tau, \nu) = 1$. For most other signals, however, the weighting function will produce a truncation of the signal's AF which corresponds to a broadening in the CWD.

2.4. The cone-kernel representation

The weighting function of the *cone-kernel representation*[3] (CKR) [21, 19, 18] is

$$\Psi_{CKR}(\tau, \nu) = g(\tau)|\tau|\mathrm{sinc}(\pi\tau\nu), \tag{4}$$

where $g(\tau)$ is a window function and $\mathrm{sinc}(\alpha) = \sin(\alpha)/\alpha$. The shape of the weighting function $\Psi_{CKR}(\tau, \nu)$ (see Fig. 2(c)) has some interesting characteristics which correspond to a very specific behavior regarding IT attenuation and TF concentration. In particular, $\Psi_{CKR}(\tau, \nu)$ is zero on the entire ν-axis,

$$\Psi_{CKR}(0, \nu) \equiv 0 ,$$

which corresponds to the fact that the CKR's integral with respect to frequency, and thus also the CKR's integral over the entire TF plane, is zero:

$$\int_f \mathrm{CKR}_x(t, f)\mathrm{d}f \equiv 0 , \quad \int_t \int_f \mathrm{CKR}_x(t, f)\mathrm{d}t\mathrm{d}f = 0 . \tag{5}$$

[3] We use the term *representation* instead of *distribution* since the cone-kernel representation is not an "energy distribution" that distributes the signal's energy over the TF plane. In fact, the TF integral is always zero (cf. Eq. (5)). This is a marked difference from the SPWD or the CWD.

Thus, the CKR is not an "energy distribution". It follows from (5) that the CKR must contain significant negative components even in those cases where the WD is (nearly) positive. Indeed, the CKR weighting function is (nearly) zero around the ν-axis, i.e., precisely where at least a part of the AF signal terms is usually located. Hence, we must expect the CKR signal terms to contain severe distortion as compared to the WD signal terms. In the case of constant-frequency signals, this distortion will be seen to be essentially a narrowing of the frequency width, accompanied by noticeable negative components. In other cases (especially chirp signals), the effects of this distortion are more troublesome (see Section 3).

It follows from (4) (specifically, from the decay of the sinc function) that the CKR will feature reasonable IT attenuation whenever ν_{12} is not near 0, i.e., whenever the interfering signal components do not occur around the same frequency. However, the opposite case $\nu_{12} \approx 0$ presents some unique features. For $\nu_{12} = 0$, we obtain

$$\Psi_{\mathrm{CKR}}(\tau, 0) = g(\tau)|\tau|,$$

which is zero for $\tau = 0$ and for $|\tau| > \frac{1}{2}T_g$ (where T_g denotes the length of the window $g(\tau)$), and will assume a maximum for $\tau = \pm\tau_0$ where τ_0 is some time lag with $0 < \tau_0 < \frac{1}{2}T_g$ (see Fig. 2(c)). Note that the two points $(-\tau_0, 0)$ and $(\tau_0, 0)$ on the τ-axis are the global maxima of $|\Psi_{\mathrm{CKR}}(\tau, \nu)|$. Thus, whenever two signal components occur around the same frequency, $\nu_{12} \approx 0$, and their time distance is near τ_0, $|\tau_{12}| \approx \tau_0$, the IT will be large. If, on the other hand, the time distance is $\frac{1}{2}T_g$ or larger, then the IT will be totally suppressed. Since $\Psi_{\mathrm{CKR}}(\tau, \nu)$ is not concentrated around the origin of the (τ, ν)-plane but rather around the two points $(-\tau_0, 0)$ and $(\tau_0, 0)$ on the τ-axis, $\Psi_{\mathrm{CKR}}(\tau, \nu)$ is the transfer function of a directional bandpass filter rather than that of a lowpass filter. This is a basic difference from the SPWD and the CWD.

3. Experimental comparison

In the previous section, the analysis of the ambiguity-domain weighting function $\Psi_T(\tau, \nu)$ yielded valuable insights into the IT attenuation and TF concentration characteristics of the SPWD, CWD, and CKR. We shall now illustrate, verify, and supplement these insights by looking at specific TFR results.

A natural question that arises in many practical applications of TFRs is, "what will a given TFR look like for a given signal under analysis?" Often, this aspect is far more immediate and important than the aspect of mathematical properties or a detailed quantitative analysis of specific effects. Therefore, in this section, we systematically compare the results of the SPWD, CWD, and CKR for some simple two-component signals. The signal components used are complex Gaussians, sinusoidal bursts, chirp (linear FM) signals, and quadratic FM signals. The signals are selected with the aim of illustrating the effects discussed in the previous section, and to highlight the strengths and weaknesses of the various TFRs. The diversity of the signals used helps to minimize any undesired bias in favor or against a specific TFR.

We have restricted our analysis to simple synthetic signals whose TF structure is known beforehand, so as to permit an assessment of the "truthfulness" of TFR results, the easy identification of specific effects, and an analysis of the TFRs' interference geometries. The insights gained from the study of these simple signals are necessary for correctly interpreting the TFR results obtained for the (usually much more complicated) real-world signals encountered in practial applications.

3.1. Experimental setup

The TFRs are displayed graphically by means of contour-line plots showing the positive TFR parts. We use 10 contour lines linearly spaced between the maximum height of the TFR surface and 0.03 times the maximum height. Compared to 3-D plots, contour-line plots are advantageous in that they clearly show the locations and spreads of signal terms and ITs in the TF plane, and thus permit an easy evaluation of a TFR's *TF concentration* and *IT geometry*. On the other hand, a disadvantage of contour-line plots is that they tend to over-emphasize components with small heights, such as small ITs. To compensate for this disadvantage, we supplement our contour-line plots by cross sections (cuts) along the time direction. Some 5 local cuts are taken around frequencies which are marked in the contour-line plots by lines labeled A, B,

and C. These cross sections give a precise indication of the IT amplitudes relative to the signal term amplitudes, i.e., of a TFR's *IT attenuation*. They also show negative components which are not (directly) visible in the contour-line plots.

The duration of all signals is 128 samples. The frequency band shown in the contour-line plots is one half of the sampling frequency. All signals are synthetic and were created directly in discrete-time format; however, in order to be closer to a real-world scenario, the time and frequency axes are labelled in ms and Hz, respectively, assuming a (hypothetical) sampling rate of 1 kHz. Thus, the TFR plots show a time interval of length 128 ms and a frequency band of 500 Hz.

The TFR parameters were chosen as follows. The SPWD windows $g(t)$ and $h(t)$ were implemented in discrete-time format using Hamming windows. To a certain extent, the window lengths L_g and L_h (controlling the amounts of time smoothing and frequency smoothing, respectively) were adapted to the respective signal. For example, a small amount of frequency smoothing was chosen in the case of an IT oscillating in the time direction only. A similar adaptation is not possible for the other two TFRs. Therefore, we used a CWD with a fixed parameter $\sigma = 30$ and a CKR with a Hamming window with fixed length (length of the discrete-time version of the window $g(\tau)$) of 41. Since these specific choices are of course questionable due to their arbitrariness, the effect of varying these parameters is studied in Section 3.7.

3.2. Two Gaussians

The closest approximation to two "TF point signals" that is permitted by the uncertainty principle is given by two Gaussian signals suitably TF-shifted to two TF points (t_1, f_1) and (t_2, f_2). Fig. 4 considers the case where the two Gaussians occur at different times ($\tau_{12} = t_1 - t_2 \neq 0$) and different frequencies ($\nu_{12} = f_1 - f_2 \neq 0$). In all three TFRs, the IT is effectively suppressed. Note, however, that the CKR shows a distortion of the signal terms involving negative parts as predicted in Section 2.4. This results in an incorrect representation of bandwidth in the CKR signal terms.

Fig. 5 again considers the case of two Gaussians, but now the Gaussians occur at the same frequency ($f_1 = f_2$ or $\nu_{12} = 0$). The SPWD's TF concentration of the signal terms is as before, but the IT is attenuated less due to the smaller distance of the interfering signal components in the TF plane. The IT attenuation could easily be improved by decreasing the window length L_h (i.e., more frequency smoothing), but this would result in poorer frequency concentration.

The CWD contains an IT with large amplitude and time spread, and thus shows a dramatic difference from the CWD result in Fig. 4. Note that this result is in perfect agreement with the theoretical discussion of Section 2.3: in the ambiguity domain, the IT falls onto the τ-axis where the CWD's weighting function $\Psi_{\mathrm{CWD}}(\tau, \nu)$ is 1 so that the IT is poorly attenuated. In the CKR, as in the previous example, the IT is effectively suppressed. Similar results (not shown) are obtained for two Gaussians located at the same time ($\tau_{12} = 0$).

Fig. 6 shows the case where the two Gaussians occur around different times and frequencies ($\tau_{12} \neq 0$ and $\nu_{12} \neq 0$) but, due to the Gaussians' large bandwidth, there is some overlap with respect to frequency. The CWD features good TF concentration but contains a noticeable residual IT in the frequency interval where the two Gaussians overlap (i.e., for all pairs of "signal points" which occur at the same frequency – cf. Section 2.3). The CKR features effective IT suppression but some distortion of the Gaussian signal terms. In particular, the bandwidth of the CKR signal terms is too small, so that the frequency overlap of the Gaussians is not shown in the CKR.

3.3. Two sinusoidal bursts

A signal consisting of two sinusoidal bursts (complex sinusoids multiplied by a rectangular window) is studied in Fig. 7. The signal components are effectively frequency-disjoint but they overlap with respect to time. In the SPWD and the CKR, the IT is effectively suppressed. The CWD, however, shows noticeable ITs in the time interval where the bursts overlap. The SPWD and CWD signal terms clearly show the local broadband characteristic of the sinusoidal bursts at the instants where the bursts are switched on or off. This (desirable) feature is much less pronounced in the CKR.

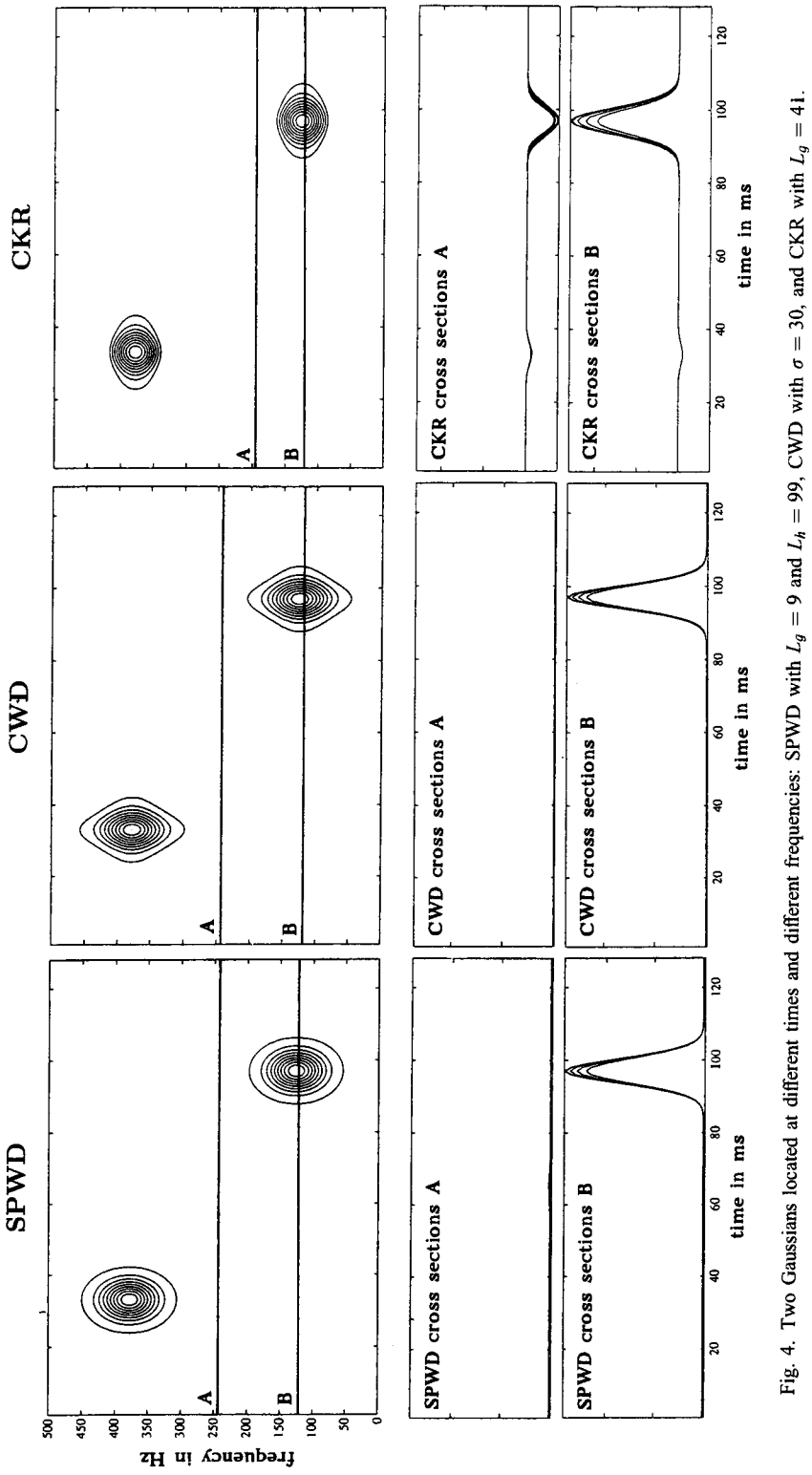

Fig. 4. Two Gaussians located at different times and different frequencies: SPWD with $L_g = 9$ and $L_h = 99$, CWD with $\sigma = 30$, and CKR with $L_g = 41$.

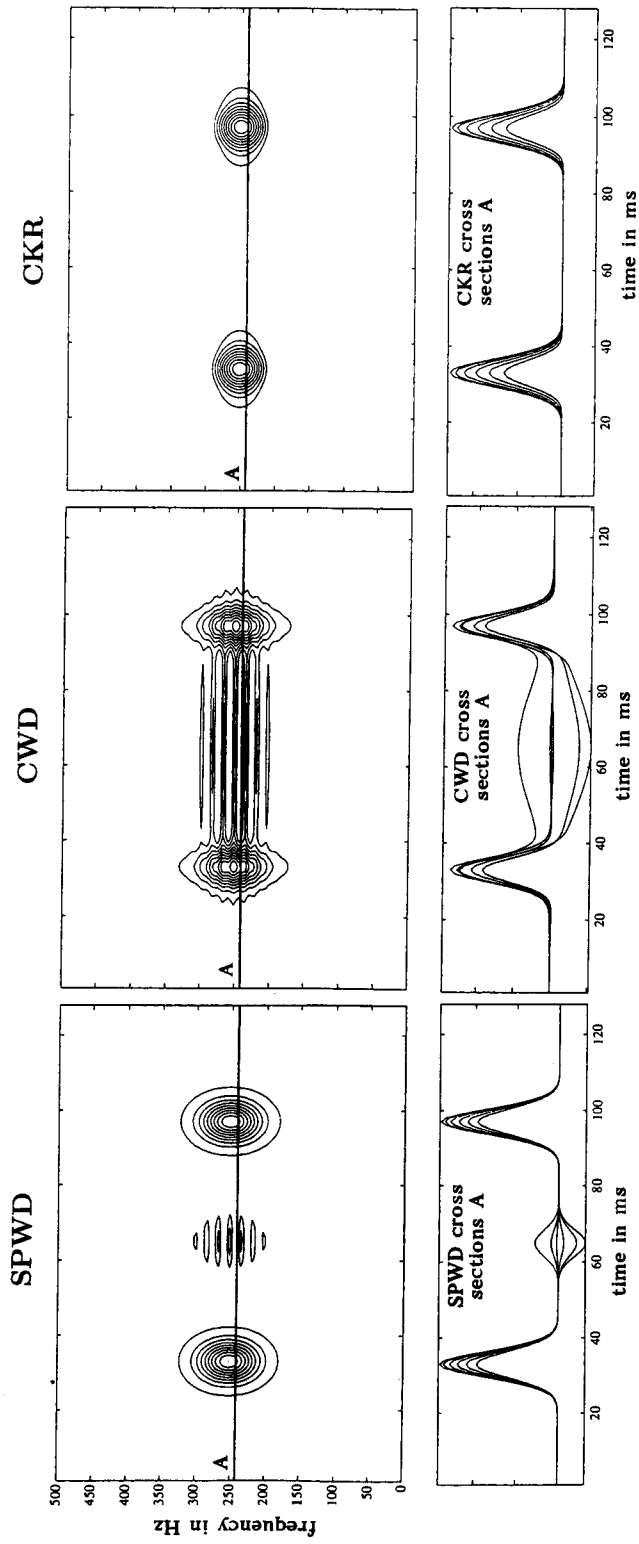

Fig. 5. Two Gaussians located at the same frequency: SPWD with $L_g = 9$ and $L_h = 99$, CWD with $\sigma = 30$, and CKR with $L_g = 41$.

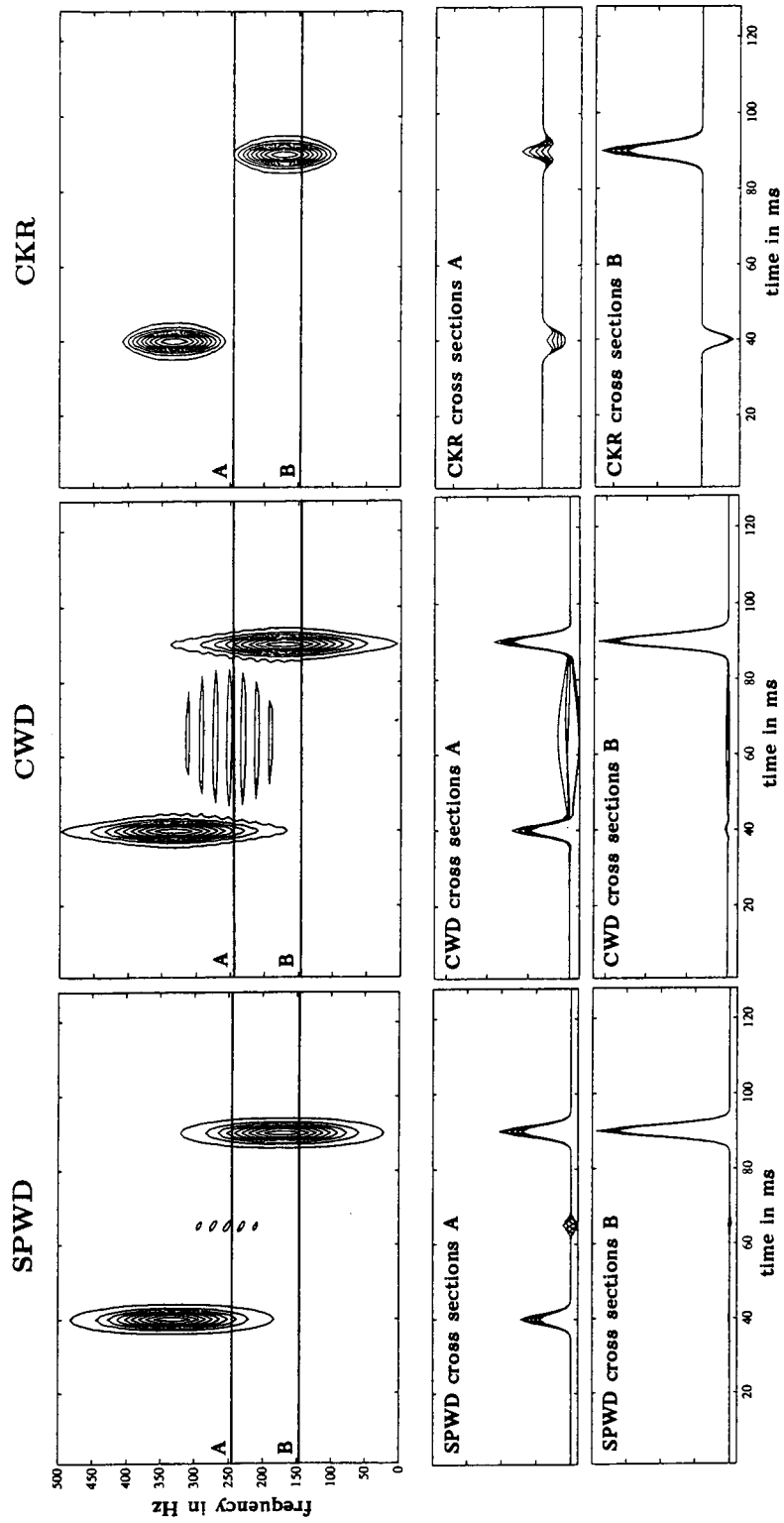

Fig. 6. Two Gaussians overlapping with respect to frequency: SPWD with $L_g = 3$ and $L_h = 63$, CWD with $\sigma = 30$, and CKR with $L_g = 41$.

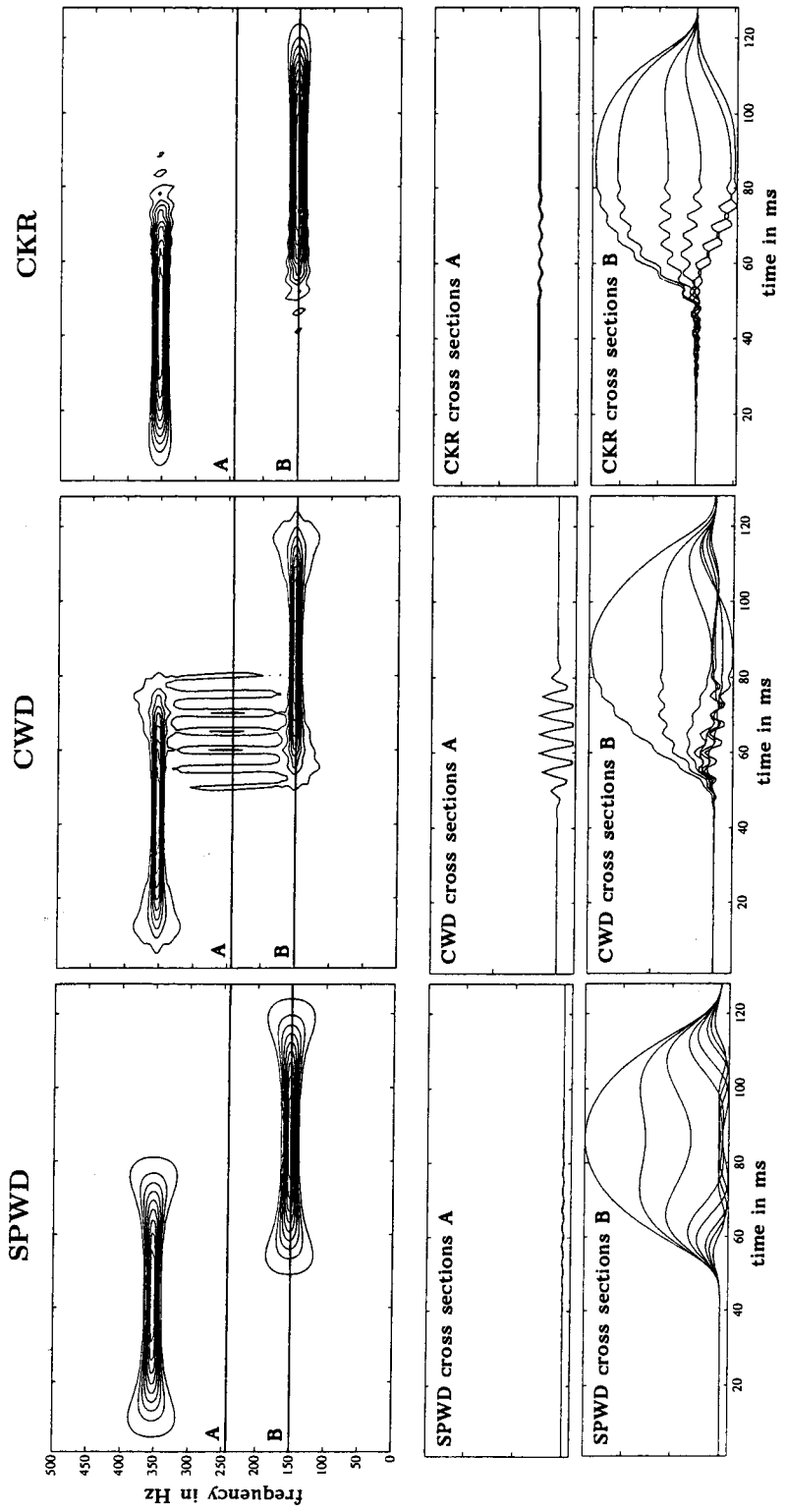

Fig. 7. Two sinusoidal bursts overlapping with respect to time: SPWD with $L_g = 15$ and $L_h = 99$, CWD with $\sigma = 30$, and CKR with $L_g = 41$.

3.4. Gaussian and chirp signal

The case of a Gaussian and a chirp signal (linear FM signal) considered in Fig. 8 is interesting since in the WD the various IT parts would oscillate in all possible directions. The SPWD shows reasonable TF concentration and good IT attenuation. Both the CWD and the CKR display the chirp signal with poorer TF concentration (as compared to the SPWD). The chirp signal term's TF concentration is especially poor in the CKR, which shows positive and negative "sidelobes". The CWD contains noticeable residual ITs between signal points located at the same time or at the same frequency.

3.5. Sinusoid and chirp signal

Fig. 9 shows the case of a sinusoidal burst and a chirp burst. The two signal components are effectively disjoint with respect to frequency but the chirp signal falls entirely into the time support of the sinusoid. The SPWD shows good overall performance, with some residual ITs in the TF region where the two signal components are closest. In the CWD, the frequency concentration of the sinusoid is excellent, which conforms to the theoretical result that the CWD's concentration is best for impulse-like signals or sinusoids (see Section 2.3). However, the residual ITs of the CWD exist over the entire time support of the chirp signal (i.e., all time points where the two signal components overlap in time). Both the CWD and the CKR display the chirp signal with poor concentration and with too small heights. Especially in the CKR, the chirp signal is grossly underrepresented. The IT attenuation in the CKR is quite good, due to the fact that the two signal components are effectively frequency-disjoint.

3.6. Gaussian and quadratic FM

Our last example, shown in Fig. 10, is that of a Gaussian and a (windowed) quadratic-FM[4] signal. In the SPWD, ITs are well attenuated and the TF concentration of the quadratic-FM component is better than in the other two TFRs. The CWD shows noticeable ITs corresponding to signal points occurring around the same time or around the same frequency; the associated ITs oscillate in the time direction and frequency direction, respectively. Finally, the CKR displays the quadratic-FM signal very poorly, except for the central time interval where the signal's frequency is locally stationary. This underlines the fact that the CKR is primarily suited for signals with quasi-constant frequency.

[4] The name "quadratic FM" refers to the signal's instantaneous frequency which is a quadratic function of time.

3.7. Variation of parameters

The effects of varying the spread parameter σ in the CWD and the length of the window $g(\tau)$ in the CKR are studied in Fig. 11 and 12, respectively. Fig. 11 shows that, as expected, a larger (smaller) σ in the CWD causes less (more) TF smoothing, which produces better (poorer) TF concentration of the signal terms but poorer (better) IT attenuation as far as the ITs' heights are concerned. For σ very large, the CWD becomes similar to the WD, which means that the signal terms are very sharp but also that the IT heights are large. For σ very small, on the other hand, the TF concentration of "chirp-like" signal components (i.e., signal components that are slanted in the TF plane) becomes very poor. Even for small σ, the CWD is still seen to contain noticeable residual ITs between signal points located around the same time or the same frequency. For small σ, the ITs' heights are reduced but their spreads are often increased.

Fig. 12 shows that the CKR results are strongly dependent on the CKR's window length L_g. A very small window length L_g yields good IT attenuation and an overall result that is somewhat similar to the SPWD result in Fig. 10. With L_g growing, the chirp-like (slanted) structures are increasingly underrepresented, and ITs between signal points located around the same frequency are appearing. In the last figure (showing the case $L_g = 127$), almost all signal terms are covered by oscillatory ITs. The mechanism of these ITs has been described in Section 2.4: as L_g is increased, the locations $(\pm\tau_0, 0)$ of the global maxima of the CKR's weighting function $|\Psi_{\mathrm{CKR}}(\tau, \nu)|$ are closer to the IT locations in the (τ, ν)-plane. On the other hand, it is also seen that the frequency concentration of constant-frequency signal terms (the central part of the quadratic FM signal) improves with growing L_g.

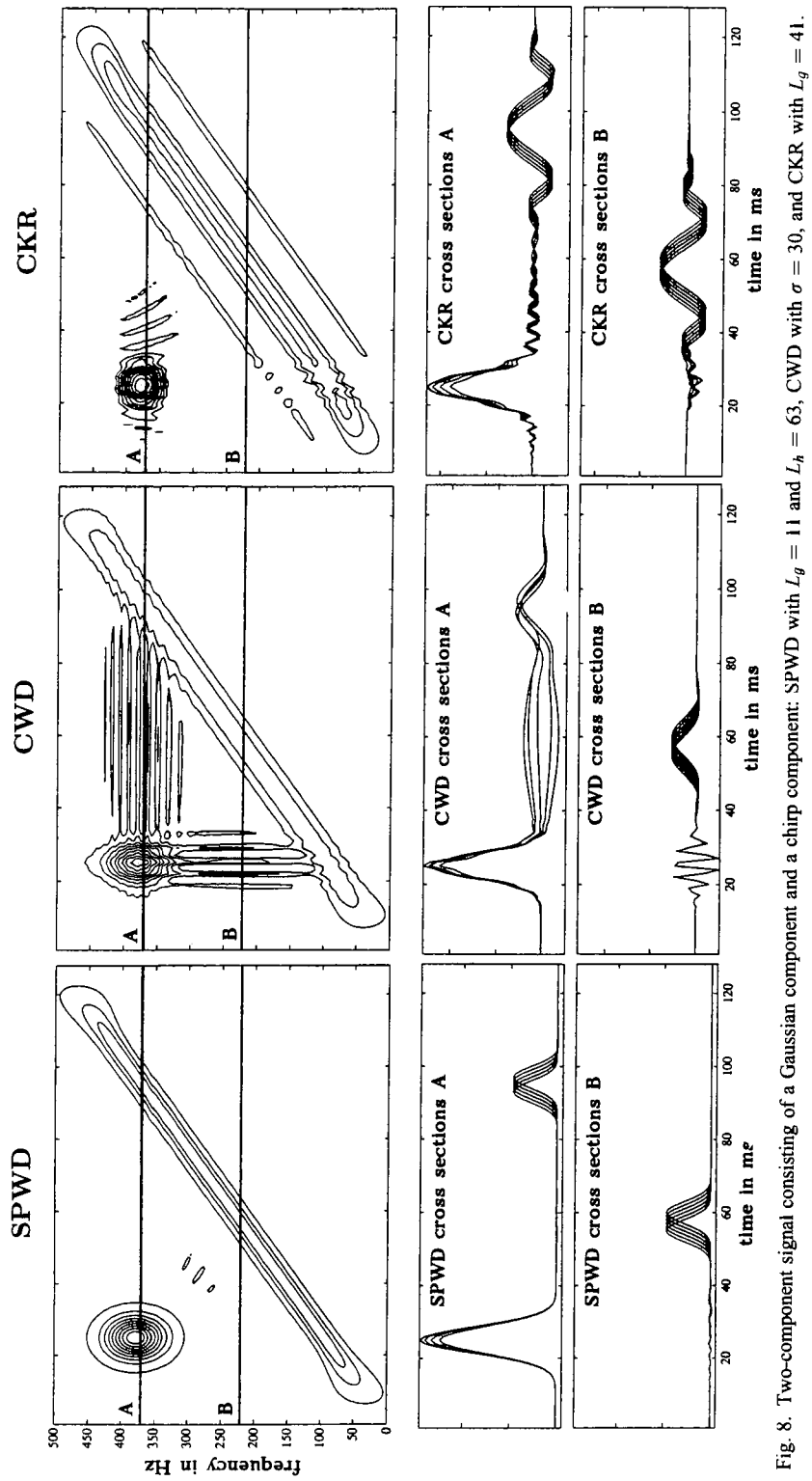

Fig. 8. Two-component signal consisting of a Gaussian component and a chirp component: SPWD with $L_g = 11$ and $L_h = 63$, CWD with $\sigma = 30$, and CKR with $L_g = 41$.

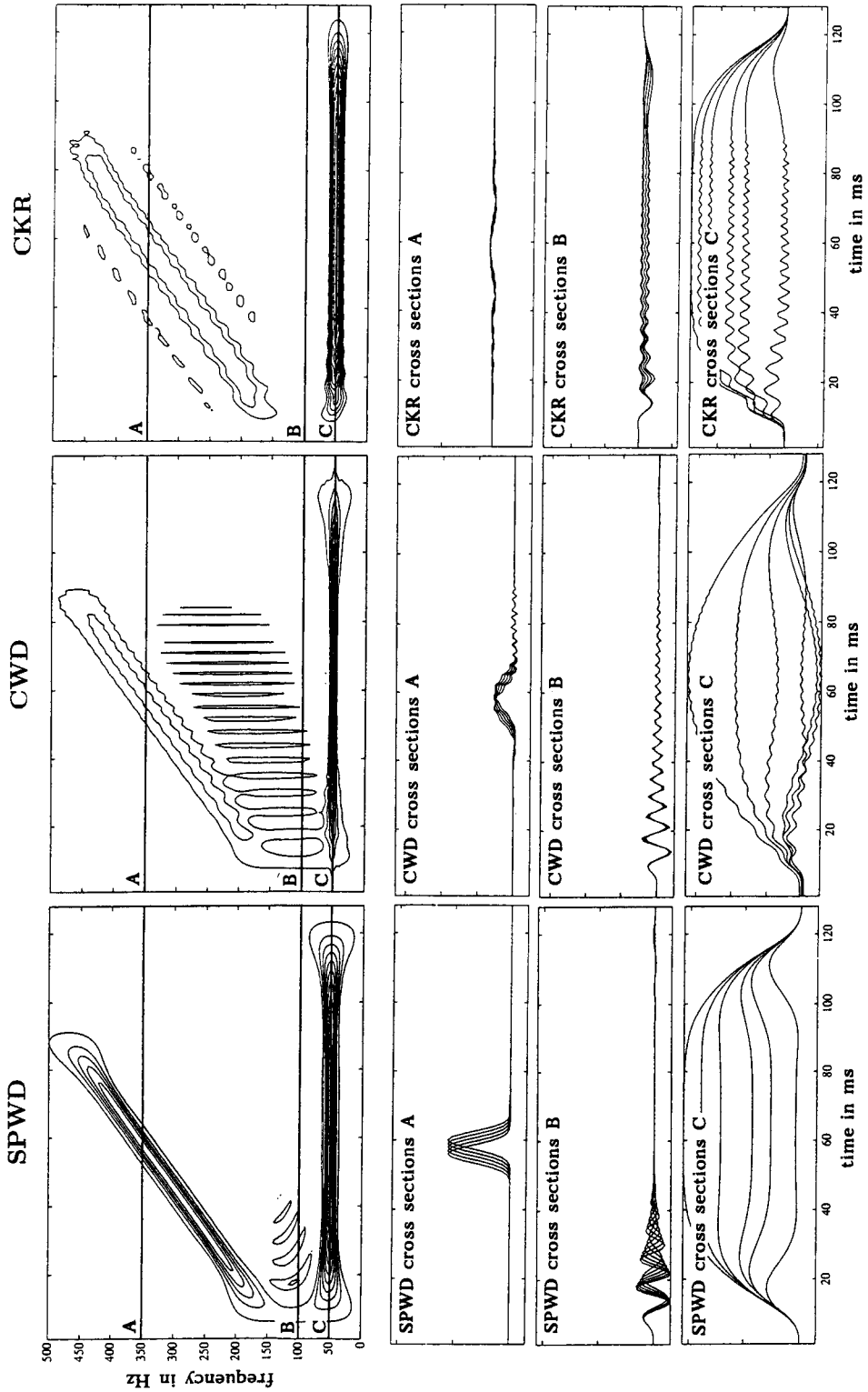

Fig. 9. Two-component signal consisting of a sinusoidal component and a chirp component: SPWD with $L_g = 11$ and $L_h = 99$, CWD with $\sigma = 30$, and CKR with $L_g = 41$.

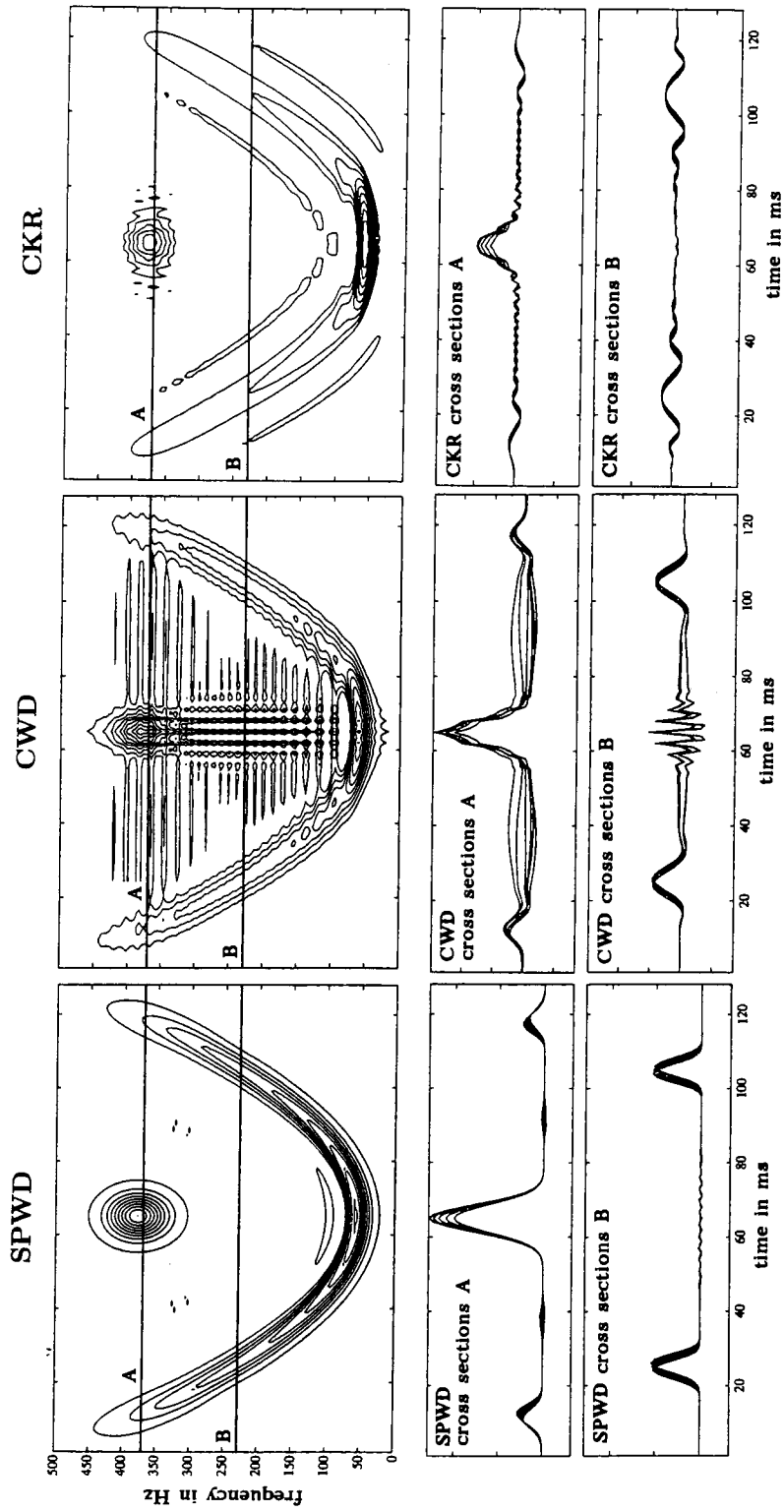

Fig. 10. Two-component signal consisting of a Gaussian component and a quadratic-FM component: SPWD with $L_g = 11$ and $L_h = 63$, CWD with $\sigma = 30$, and CKR with $L_g = 41$.

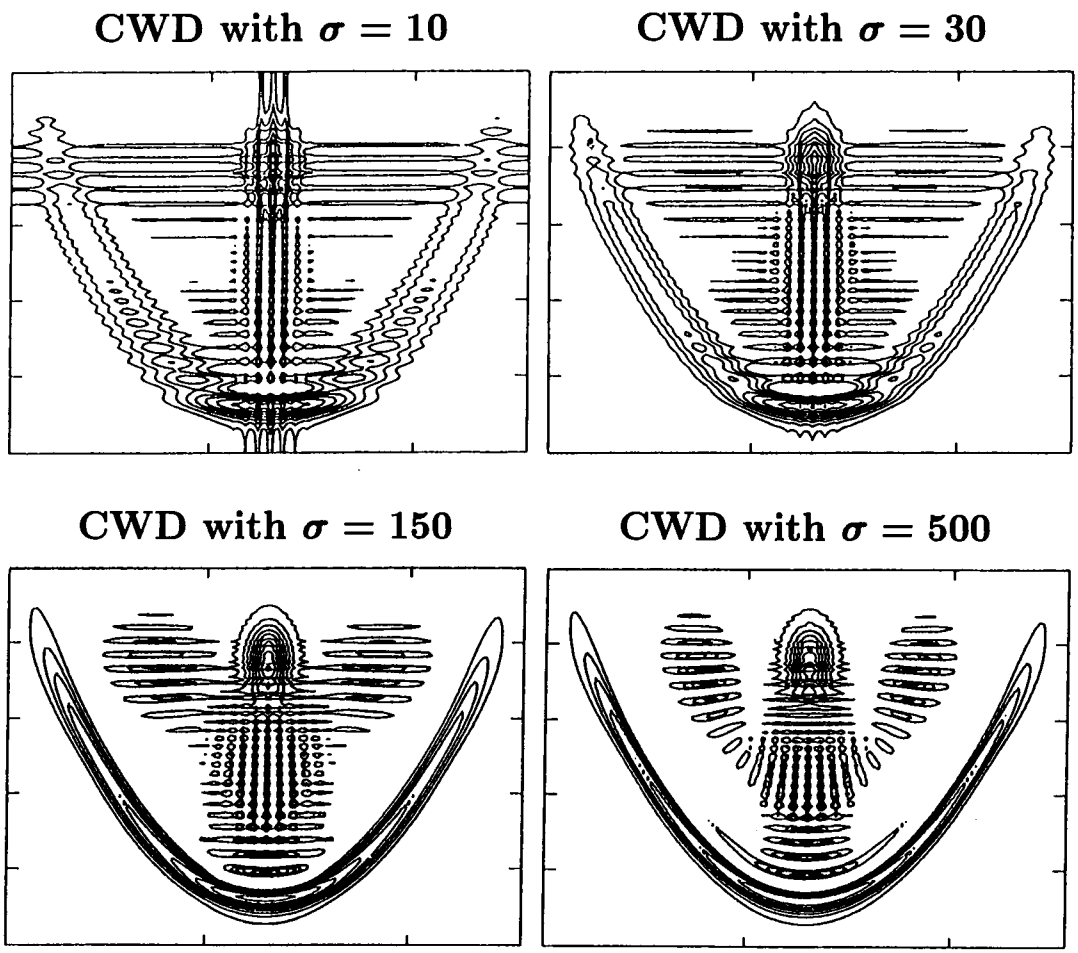

Fig. 11. Effects of varying the spread parameter σ in the CWD. The plots show CWDs of the signal previously considered in Fig. 10, with CWD spread parameter $\sigma = 10$, $\sigma = 30$, $\sigma = 150$, and $\sigma = 500$, respectively.

4. Conclusion

We have compared the time–frequency (TF) concentration and interference-term (IT) attenuation characteristics of three TF representations known as the smoothed pseudo-Wigner distribution (SPWD), the Choi–Williams distribution (CWD), and the cone-kernel representation (CKR). Our discussion of these characteristics was based on an analysis of the shape of the ambiguity-domain weighting function and on the results obtained for some simple but representative, two-component signals.

It was found that the "simple" smoothing employed by the SPWD leads to a reliable and stable IT attenuation as well as reasonably good TF concentration. "Stability" of the IT attenuation means that, excluding extreme choices of the two window lengths controlling the SPWD smoothing, the SPWD's IT attenuation does not depend too much on the type of the signal, besides the unavoidable dependence on the TF distance between the interfering signal components. On the other hand, the SPWD does not satisfy most of the desirable mathematical properties like the marginal or finite-support properties.

The CWD satisfies a large number of mathematical properties. It achieves potentially better TF concentration than the SPWD for impulsive signals or sinusoids with quasi-constant frequency (signals which, in the TF plane, are parallel to the time or frequency axis), but not for "chirp-like" signals (which are slanted in

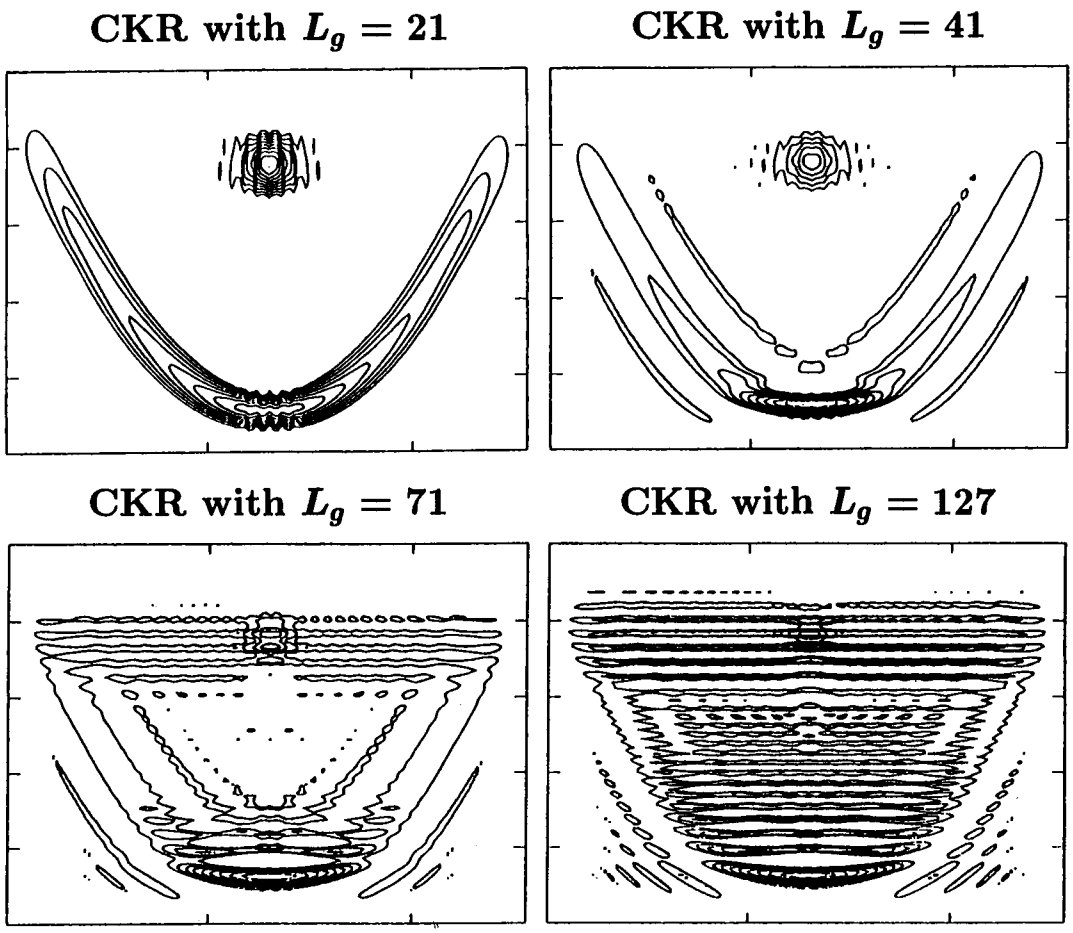

Fig. 12. Effects of varying the window length parameter L_g in the CKR. The plots show the CKR of the signal previously considered in Fig. 10, with CKR window length $L_g = 21$, $L_g = 41$, $L_g = 71$, and $L_g = 127$, respectively.

the TF plane). The CWD's IT attenuation exhibits a strong dependence on the signal's TF structure. It is potentially poor if the signal components overlap in time or in frequency: in the overlap intervals, any reduction of IT amplitude comes at the cost of a proportional increase of IT spread. Such a behavior is necessary for the marginal properties to be satisfied.

The CKR yields good results for signals consisting of sinusoidal bursts with quasi-constant frequency. However, if the CKR's window is not small enough, the CKR's IT attenuation is potentially poor for signal components overlapping in frequency. On the other hand, a smaller window entails poorer frequency concentration for signals with quasi-constant frequency. Like the CWD, the CKR is less suited for chirp-like signals. The negative parts of CKR signal terms are often significant and may cause signals to be represented with too small bandwidths if only the positive CKR parts are plotted.

References

[1] B. Boashash, "Time–frequency signal analysis", in: S. Haykin, ed., *Advances in Spectrum Estimation*, Prentice-Hall, Englewood Cliffs, NJ, 1990.

[2] H.-I. Choi and W.J. Williams, "Improved time–frequency representation of multicomponent signals using exponential kernels", *IEEE Trans. Acoust. Speech Signal Process.*, Vol. ASSP-37, June 1989, pp. 862–871.

[3] T.A.C.M. Claasen and W.F.G. Mecklenbräuker, "The Wigner distribution – A tool for time–frequency signal analysis", Parts I–III, *Philips J. Res.*, Vol. 35, 1980, pp. 217–250, 276–300, 372–389.

[4] L. Cohen, "Time–frequency distributions – A review", *Proc. IEEE*, Vol. 77, No. 7, July 1989, pp. 941–981.

[5] A.H. Costa and G.F. Boudreaux-Bartels, "Design of time–frequency representations using a multiform, tiltable exponential kernel", *IEEE Trans. Signal Process.*, To appear.

[6] P. Flandrin, "Some features of time–frequency representations of multicomponent signals", *Proc. IEEE 1984 Internat.* Conf. Acoust. Speech Signal Processing (ICASSP-84), San Diego, CA, March 1984, pp. 41B.4.1-41B.4.4.

[7] P. Flandrin, *Temps–Fréquence*, Hermès, Paris, 1993.

[8] P. Flandrin and W. Martin, "Pseudo-Wigner estimators for the analysis of nonstationary processes", *Proc. IEEE Spectr. Est. Workshop II*, Tampa, FL, November 1983, pp. 181–185.

[9] H. Garudadri and E. Velez, "A comparison of smoothing kernels for computing bilinear time–frequency representations", *Proc. IEEE 1991 Internat. Conf. Acoust. Speech Signal Processing (ICASSP-91)*, Toronto, Canada, May 1991, pp. 3221–3224.

[10] C. Griffin and A.H. Nuttall, "Comparison of two kernels for the modified Wigner distribution function", Society of Photo-Optical Instrumentation Engineers, San Diego, CA, July 1991.

[11] F. Hlawatsch, "Duality and classification of bilinear time–frequency signal representations", *IEEE Trans. Signal Process.*, Vol. 39, No. 7, July 1991, pp. 1564–1574.

[12] F. Hlawatsch and G.F. Boudreaux-Bartels, "Linear and quadratic time–frequency signal representations", *IEEE Signal Process. Mag.*, Vol. 9, No. 2, April 1992, pp. 21–67.

[13] F. Hlawatsch and P. Flandrin, "The interference structure of the Wigner distribution and related time–frequency signal representations", in: W. Mecklenbräuker, ed., *The Wigner Distribution – Theory and Applications in Signal Processing*, Elsevier, Amsterdam, 1995, To appear.

[14] F. Hlawatsch and R.L. Urbanke, "Bilinear time–frequency representations of signals: The shift-scale invariant class", *IEEE Trans. Signal Process.*, Vol. 42, No. 2, February 1994, pp. 357–366.

[15] A.J.E.M. Janssen, "On the locus and spread of pseudo-density functions in the time–frequency plane", *Philips J. Res.*, Vol. 37, No. 3, 1982, pp. 79–110.

[16] J. Jeong and W.J. Williams, "Kernel design for reduced interference distributions", *IEEE Trans. Signal Process.*, Vol. 40, No. 2, February 1992, pp. 402–412.

[17] D.L. Jones and T.W. Parks, "A resolution comparison of several time–frequency representations", *IEEE Trans. Signal Process.*, Vol. 40, No. 2, February 1992, pp. 413–420.

[18] P.J. Loughlin, J.W. Pitton and L.E. Atlas, "Bilinear time–frequency representations: New insights and properties", *IEEE Trans. Signal Process.*, Vol. 41, No. 2, February 1993, pp. 750–767.

[19] S. Oh and R.J. Marks, II, "Some properties of the generalized time–frequency representation with cone-shaped kernel", *IEEE Trans. Signal Process.*, Vol. 40, No. 7, July 1992, pp. 1735–1745.

[20] A. Papandreou and G.F. Boudreaux-Bartels, "Generalization of the Choi–Williams distribution and the Butterworth distribution for time–frequency analysis", *IEEE Trans. Signal Process.*, Vol. 41, No. 1, January 1993, pp. 463–472.

[21] Y. Zhao, L.E. Atlas and R.J. Marks, II, "The use of cone-shaped kernels for generalized time–frequency representations of nonstationary signals", *IEEE Trans. Acoust. Speech Signal Process.*, Vol. ASSP-38, July 1990, pp. 1084–1091.